

## MULTISCALE TEXTURE RECOGNITION USING ANISOTROPIC DIFFUSION-BASED SCALE SPACE AND COMBINED ROTATION-INVARIANT FEATURE DESCRIPTORS

Tudor BARBU<sup>1</sup>, Paul UNGUREANU<sup>2</sup>, Liviu GORAȘ<sup>2,1</sup>

<sup>1</sup> Institute of Computer Science, Romanian Academy – Iași Branch

<sup>2</sup> “Gheorghe Asachi” Technical University of Iasi, Romania

Corresponding author: Tudor BARBU, E-mail: tudor.barbu@iit.academiaromana-is.ro

**Abstract.** A novel multi-scale image analysis framework for rotation-invariant texture recognition is proposed in this article. A well-posed second-order nonlinear anisotropic diffusion-based model is proposed and a scale-space representation is then constructed by applying the finite difference-based numerical approximation algorithm of this PDE-based model on the current image. A texture feature extraction combining gray level co-occurrence matrices (GLCM) and 2D circular filters is performed at each scale. The feature descriptors computed at multiple scales are then concatenated into the final rotation-invariant texture feature vector. Next, the feature vectors are classified applying supervised machine learning algorithms, such as K-NN, and using texture training sets. Last but not least, texture recognition experiments and method comparison are also discussed.

**Key words:** multiscale texture analysis, nonlinear anisotropic diffusion-based model, numerical approximation scheme, Gray Level Co-occurrence Matrix, circular filters, texture feature vector, supervised machine learning algorithm.

### 1. INTRODUCTION

The notion of texture denotes images in which a specific pattern of distribution and dispersion of the pixel intensity is repeated sequentially throughout them. Texture analysis represents an important image processing domain that has numerous computer vision application areas, such as: object detection, recognition and tracking, image indexing and retrieval, medical imaging, product quality diagnosis and remote sensing. It includes several image analysis fields, such as the texture recognition, segmentation, synthesis and retrieval.

Texture recognition consists of two main phases: texture feature extraction and classification. The existing texture featuring techniques can be grouped in the following categories: statistical, structural, model-based and transform-based approaches. Statistical methods include histogram-based algorithms [1], moment-based solutions [2], Gray Level Co-occurrence Matrices (GLCM) [3], Local Binary Patterns (LBP) [4], Binary Gabor Patterns (BGP) [5] and energy variation-based methods [6]. The structural techniques include edge-based algorithms [7], morphological operators [8] and SIFT descriptors [9]. Model-based approaches include fractal texture models [10], Markov random field texture models [11] and autoregressive models [12]. Transform-based techniques include texture feature extraction methods based on 2D Gabor filters [13], Wavelet transforms [14] and Curvelet transforms [15]. Some other effective methods combining these texture descriptors have been developed as well [16].

Depending on the character of the texture recognition process, supervised or unsupervised texture feature vector classification approaches can be applied [17]. Thus, supervised machine learning algorithms that can be used for texture classification include *K*-Nearest Neighbour (*K*-NN), minimum distance classifier, artificial neural networks (ANN), Support Vector Machines (SVM) and Hidden Markov Models (HMM), while the unsupervised classification techniques include *K*-means, hierarchical clustering, Self-organizing Maps (SOM) and Dynamic Time Warping (DTW). Deep learning schemes have been also used successfully for texture classification [18].

Most texture recognition techniques provide weaker classification rates when textures have undergone rotations and also their performances are affected by image noise. So, a novel rotation-invariant supervised texture recognition framework based on multiscale image analysis, which works properly in both normal and noisy conditions, is proposed in this research paper. An anisotropic diffusion-based scale space is constructed by using the finite difference method-based numerical approximation algorithm of the nonlinear second-order diffusion model introduced in the next section. Then, a texture feature extraction is performed at each scale and a final texture descriptor is obtained by concatenating all the feature vectors achieved at multiple scales. The proposed texture feature extraction technique that combines Gray Level Co-occurrence Matrices to circular filters is described in the third section. The supervised texture classification approach, which is also presented in that section, is based on a  $K$ -NN classifier.

The results achieved by the proposed texture recognition technique and illustrating its effectiveness are discussed in the fourth section. Our approach outperforms many well-known texture recognition methods and, unlike them, it is also able to successfully recognize rotated textures. The conclusions of this work are drawn in the last section.

## 2. NONLINEAR ANISOTROPIC DIFFUSION-BASED SCALE SPACE REPRESENTATION

Multi-scale and multi-resolution image analysis approaches, which handle image structures at different scales and resolutions, are successfully used in many image processing and computer vision fields, such as edge, corner and blob detection or texture analysis, since the multi-scale and multi-resolution representations allow more flexibility and provide better results than the traditional techniques. A scale space representation is obtained by applying a 2D filter kernel to the analysed image at various scales. While many multiscale image and texture analysis solutions use scale spaces based on 2D Gaussian kernels and Gaussian derivatives [19], we propose a more effective scale-space representation based on anisotropic diffusion-based filtering. Thus, a nonlinear second-order anisotropic diffusion model is introduced in the first subsection, then its numerical discretization is used to construct the scale space.

### 2.1. A compound second-order parabolic PDE-based filter

We have developed several partial differential equation (PDE) models for image processing and analysis in the past [20, 21]. Here we propose a novel second-order anisotropic diffusion-based model for constructing the scale space representation. It is composed of a nonlinear parabolic PDE and its boundary conditions, having the following form:

$$\begin{cases} \frac{\partial u}{\partial t} - \alpha \varphi(|\Delta u_\sigma|) \nabla \cdot (\psi(\|\nabla u_\sigma\|) \nabla u) + \lambda(u - u_0) = 0, & (x, y) \in \Omega \\ u(0, x, y) = u_0(x, y), & \forall (x, y) \in \Omega \\ u(t, x, y) = 0, & \forall (x, y) \in \partial\Omega \end{cases} \quad (1)$$

where the image domain is  $\Omega \subseteq \mathbb{R}^2$ , the observed image  $u_0 \in L^2(\Omega)$ ,  $u_\sigma = u * G_\sigma$ , the 2D Gaussian kernel

$G_\sigma(x, y) = \frac{1}{2\pi\sigma^2} e^{-\frac{x^2+y^2}{2\sigma^2}}$  and parameters  $\alpha \in [1, 2)$ ,  $\lambda \in (0, 1)$ . The following diffusivity function that is positive, monotonic decreasing and converging to 0 is considered for this model:

$$\psi: [0, \infty) \rightarrow [0, \infty), \quad \psi(s) = \left( \frac{\eta}{|\delta \log_{10}(\eta) + \xi s^k|} \right)^{\frac{1}{k+1}}, \quad (2)$$

where  $\delta, \xi \in (0, 1]$ ,  $\eta \geq 15$  and  $k \geq 1$ . The other positive function used within this diffusion-based model has the form:

$$\varphi : [0, \infty) \rightarrow [0, \infty), \varphi(s) = \zeta r^{+1} \sqrt{\gamma s^r + \beta}, \tag{3}$$

where  $\zeta, \gamma, \beta \in [1, 4)$  and  $r \in (0, 1)$ . The term  $\varphi(|\nabla^2 u_\sigma|)$  is introduced to control the speed of the diffusion process and enhance the essential image details.

The proposed nonlinear PDE-based model is a compound filter combining the anisotropic diffusion to a 2D Gaussian filter kernel so that to work properly in noisy conditions. It filters successfully the white additive noise while preserving and sharpening the edges and other details, and overcoming the unintended effects. It is non-variational and well-posed, since it admits a unique variational (weak) solution, which can be determined numerically constructing a numerical approximation scheme for (1) that converges to it. This discretization algorithm and the scale space representation determined by it are described in next subsection.

### 2.2. Scale-space representation using finite difference-based numerical approximation scheme

A numerical approximation algorithm is developed for the proposed diffusion model by applying the finite difference method [22]. Thus, one considers a grid of space size  $h$  and time step  $\Delta t$  for this task. The spatial coordinates are quantized as  $x = ih, y = jh, i \in \{1, \dots, I\}, j \in \{1, \dots, J\}$  and the time coordinate is quantized as  $t = n\Delta t, n \in \{0, \dots, N\}$ , where  $[Ih \times Jh]$  is the size of the support image. The PDE in (1) can be written as:

$$\frac{\partial u}{\partial t} + \lambda(u - u_0) = \alpha \varphi(|\nabla^2 u_\sigma|) \operatorname{div}(\psi(\|\nabla u_\sigma\|) \nabla u). \tag{4}$$

The left term of equation (4) is then discretized, by applying central differences [22], as:

$$\frac{u_{i,j}^{n+\Delta t} - u_{i,j}^n}{\Delta t} + \lambda(u_{i,j}^n - u_{i,j}^0) = u_{i,j}^{n+\Delta t} \frac{1}{\Delta t} + u_{i,j}^n \left( \lambda - \frac{1}{\Delta t} \right) - u_{i,j}^0 \lambda. \tag{5}$$

The right term of the equation is then approximated. The component  $\varphi(|\nabla^2 u_\sigma|)$  is discretized as  $\varphi\left(\frac{(u_\sigma)_{i+h,j}^n + (u_\sigma)_{i-h,j}^n + (u_\sigma)_{i,j+h}^n + (u_\sigma)_{i,j-h}^n - 4(u_\sigma)_{i,j}^n}{h^2}\right)$ . Then, the divergence term  $\operatorname{div}(\psi(\|\nabla u_\sigma\|) \nabla u)$  is

approximated as  $\frac{1}{4} \left[ \begin{aligned} &\psi\left(\|(u_\sigma)_{i+h,j}^n - (u_\sigma)_{\sigma i,j}^n\|\right)(u_{i+h,j}^n - u_{i,j}^n) + \psi\left(\|(u_\sigma)_{i-h,j}^n - (u_\sigma)_{i,j}^n\|\right)(u_{i-h,j}^n - u_{i,j}^n) + \\ &+ \psi\left(\|(u_\sigma)_{i,j+h}^n - (u_\sigma)_{i,j}^n\|\right)(u_{i,j+h}^n - u_{i,j}^n) + \psi\left(\|(u_\sigma)_{i,j-h}^n - (u_\sigma)_{i,j}^n\|\right)(u_{i,j-h}^n - u_{i,j}^n) \end{aligned} \right].$

We adopted the parameter values  $h = \Delta t = 1$ . The next iterative explicit numerical approximation scheme is obtained:

$$u_{i,j}^{n+1} = u_{i,j}^n (1 - \lambda) + u_{i,j}^0 \lambda + \alpha \frac{\varphi\left(\frac{(u_\sigma)_{i+1,j}^n + (u_\sigma)_{i-1,j}^n + (u_\sigma)_{i,j+1}^n + (u_\sigma)_{i,j-1}^n - 4(u_\sigma)_{i,j}^n}{4}\right) \times \left[ \begin{aligned} &\psi\left(\|(u_\sigma)_{i+h,j}^n - (u_\sigma)_{\sigma i,j}^n\|\right)(u_{i+h,j}^n - u_{i,j}^n) + \psi\left(\|(u_\sigma)_{i-h,j}^n - (u_\sigma)_{i,j}^n\|\right)(u_{i-h,j}^n - u_{i,j}^n) + \\ &+ \psi\left(\|(u_\sigma)_{i,j+h}^n - (u_\sigma)_{i,j}^n\|\right)(u_{i,j+h}^n - u_{i,j}^n) + \psi\left(\|(u_\sigma)_{i,j-h}^n - (u_\sigma)_{i,j}^n\|\right)(u_{i,j-h}^n - u_{i,j}^n) \end{aligned} \right]}{4} \tag{6}$$

The iterative numerical discretization algorithm (6) is stable and consistent to the nonlinear second-order PDE-based model (1) and converges quite fast to its variational solution representing the filtered image. The metrics of the convergence is measured as number of iterations. The scale space is then constructed by applying this numerical approximation scheme on the current texture  $u^0$  at various iterations.

So, a proper scale-space representation is produced by filtering the texture image, using the anisotropic diffusion-based model (1), until some properly selected moments of time  $t$ , and then differencing the consecutive filtered textures.

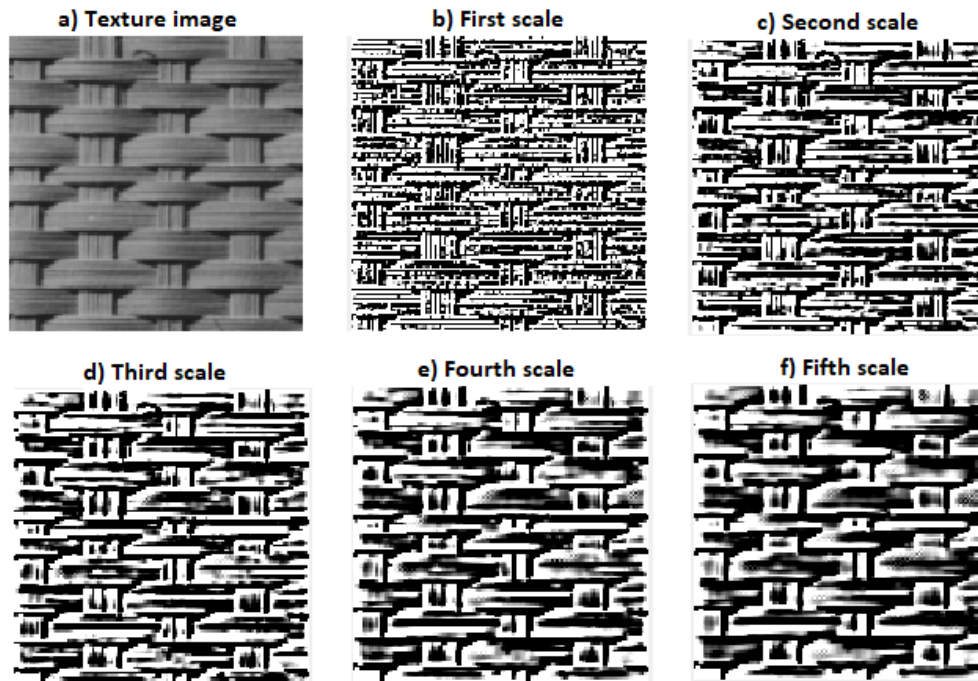


Fig. 1 – Anisotropic diffusion-based scale space ( $K = 5$ ).

So, one considers the filtering results produced by the numerical algorithm (6) at the iteration moments  $4n$ ,  $n \in \{0, \dots, K\}$ ,  $K \geq 4$ . The obtained subtraction results,  $\{u^0 - u^4, u^4 - u^8, \dots, u^{4(K-1)} - u^{4K}\}$ , constitute the scale-space representation with  $K$  scales. The image at each scale  $m \in \{1, \dots, K\}$ , which is denoted as  $U_m = u^{4(m-1)} - u^{4m}$ , represents the textural component of the PDE-based decomposition of  $u^{4(m-1)}$  and contains contours of the evolving image  $u$ . These  $K$  contour-based images are very useful for the texture analysis of the observation  $u_0$ .

An example of scale-space representation produced by our anisotropic diffusion-based approach for  $K = 5$  is provided in Fig. 1. The scale space corresponding to the texture displayed in a) is described in b)–f).

### 3. ROTATION-INVARIANT TEXTURE FEATURE EXTRACTION AND CLASSIFICATION

An effective rotation-invariant texture feature descriptor is determined by using the described scale space. Thus, a texture feature extraction process is performed for the current image at multiple scales. The proposed feature extraction technique consists in combining Gray Level Co-occurrence Matrices (GLCMs) to 2D circular filters.

The co-occurrence matrix of a given image  $u$  computes the occurrences of the pairs of pixels with a specific value and offset in that image [3] and is based on the formula:

$$CM_{\Delta x, \Delta y}[u](i, j) = \sum_x \sum_y \begin{cases} 1, & \text{for } u(x, y) = i \ \& \ u(x + \Delta x, y + \Delta y) = j \\ 0, & \text{otherwise} \end{cases} \quad (7)$$

where  $(\Delta x, \Delta y)$  represents the offset. If  $\{(\Delta x_1, \Delta y_1), \dots, (\Delta x_p, \Delta y_p)\}$  is a properly selected set of offsets, the sequence of GLCMs corresponding to that image is computed as:

$$CM(u) = \{CM_{\Delta x_1, \Delta y_1}(u), \dots, CM_{\Delta x_p, \Delta y_p}(u)\} \quad (8)$$

A GLCM-based featuring process is then performed on the observed image  $u_0$ , by applying (8) to the anisotropic diffusion-based scale-space constructed for this image. Thus, one obtains the sequence  $\{CM(U_1), CM(U_2), \dots, CM(U_K)\}$  for it. Then, a circular filtering process is applied to the images of each  $CM(U_i), i \in \{1, K\}$ .

The most popular 2D circular filters are based on the use of the Gabor filter which is described by the Fourier transform function [23, 24], as follows:

$$H_\sigma(\omega) = e^{-\frac{(\omega - \frac{\pi}{\sigma})(\mu\sigma)^2}{2}} \quad (9)$$

where  $\frac{\pi}{\sigma}$  and  $\mu\sigma$  represents the central frequency and the filter bandwidth respectively. Using the change of variable  $\omega \rightarrow \sqrt{\omega_x^2 + \omega_y^2}$ , the following transform is obtained:

$$H_\sigma(\omega_x, \omega_y) = e^{-\frac{(\sqrt{\omega_x^2 + \omega_y^2} - \frac{\pi}{\sigma})(\mu\sigma)^2}{2}}. \quad (10)$$

The main advantage of the circular filters is related to the fact that from a rotated texture with a certain angle results a texture with the same module of the Fourier transform. Thus, for a texture and its rotated version filtered with the same circular filter will result two images with the same  $L1$  or  $L2$  norms [23].

So, a bank of  $M$  such 2D filters with circular frequency response is applied to the GLCM-based images related to the scale space. Some proper values for the mean  $\mu$  and standard deviation  $\sigma$  parameters were chosen so that to produce optimal classification results. Each filter is characterized by  $\sigma = a^q, q \in \{1, \dots, M\}$ , where  $a > 1$ . Such a bank, consisting of five circular filters and the parameters  $\mu = 1.3$  and  $a = 1.6$ , is presented in Fig. 2b. Each  $CM_{\Delta x_j, \Delta y_j}(U_i), i = 1, \dots, K, j = 1, \dots, p$  image computed by (7) is mean normalized first, then convolved to each of the  $M$  two-dimension circular filters of the bank. The  $L2$  norm is next computed for each of the resulted  $M$  filtered images. Thus, an  $M$  dimensional vector composed of these norms is obtained for each  $CM_{\Delta x_j, \Delta y_j}(U_i)$ , which means  $p$  such  $M$  dimensional vectors are computed for  $U_i$ . They are then concatenated into a  $pM$  dimensional 1D feature vector,  $V(U_i)$ , but 2D  $[p \times M]$  versions of this feature vector corresponding to the  $i^{\text{th}}$  scale can be created as well. Next, these  $K$  texture feature vectors  $V(U_i)$  determined at multiple scales are combined into a final texture feature vector corresponding to the initial texture  $u_0$ . Thus, a 1D  $pMK$  dimensional feature vector is obtained for it by concatenating the feature vectors at all scales:  $V(u_0) = [V(U_1) V(U_2) \dots V(U_K)]$ . 2D ( $[pM \times K]$ ) or even 3D ( $[p \times M \times K]$ ) forms can be obtained for  $V(u_0)$  too. This feature vector represents a robust rotation-invariant and noise-insensitive texture descriptor. The pseudocode of this texture feature extraction technique is described in Fig. 2a.

A supervised texture classification process is then performed by using these feature vectors. A  $K$ -Nearest Neighbour ( $K$ -NN) classifier with a large training set containing textures grouped in some known classes is used for this purpose [17]. Each input texture is assigned to the class most common among its  $K_{NN}$  nearest neighbors. Euclidean metric is used to determine the distances between input texture feature vectors and the training feature vectors. While the training textures used in this process are noise-free and not rotated, the input textures could be noisy and rotated in order to evaluate the effectiveness of the proposed approach. The results of the recognition experiments using these texture feature vectors are discussed next.

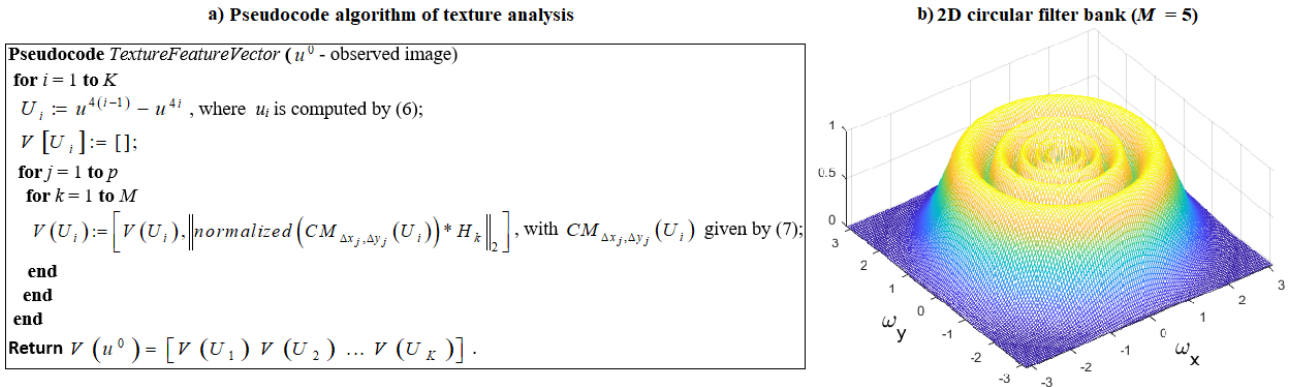


Fig. 2 – The pseudocode of the proposed texture analysis procedure and the 2D circular filter bank ( $M = 5$ ) used by it.

#### 4. TEXTURE RECOGNITION EXPERIMENTS AND METHOD COMPARISON

The proposed multiscale recognition framework has been tested successfully on thousands of normal and rotated textures. Thus, some voluminous texture image databases, such as the Brodatz album [25] and the Kylberg texture dataset [26], have been used to test the performance of our technique. The recognition experiments have been performed on Intel (R) Core (TM) i7-6700HQ CPU 2.60 GHz processor on 64 bits, operating Windows 10. The implementation of the numerical algorithms has been performed using Matlab.

The proposed technique's parameters that provide the best recognition results have been determined empirically, by applying the trial and error method. So, the identified parameters are the following ones: the number of scales  $K=5$ , the number of circular filters  $M=5$ , the number of neighbors  $K_{NN}=7$ , the set of  $(\Delta x, \Delta y)$  offsets =  $\{(0, 1), (0, 2), (-1, 1), (-2, 2), (-1, 0), (-2, 0), (-1, -1), (-2, -2)\}$ ,  $\mu = 1.3$  and  $\sigma = 1.6^q$ . Moreover, the 1D form of texture feature vectors, with 200 coefficients, leads to better classification output.

We considered 15 texture classes of Brodatz database (<http://sipi.usc.edu/database>), each one containing 280  $[128 \times 128]$  textures oriented at  $0^\circ, 20^\circ, 30^\circ, 45^\circ, 60^\circ, 70^\circ, 90^\circ, 120^\circ, 135^\circ, 150^\circ$  (28 textures for each angle), and 12 texture classes of the Kylberg collection (<https://kylberg.org/kylberg-sintorn-rotation-dataset>), each one containing 240  $[576 \times 576]$  textures at 12 orientations (20 for each angle), for our experiments. The training set of the  $K$ -NN classifier has been composed of 105 non-rotated textures, representing 7 images with  $0^\circ$  orientation from each class, for the tests involving the Brodatz image set. The experiments using the Kylberg database have used a training texture set of 84 images, representing 7 textures at  $0^\circ$  angle from each class. The texture classes used in our tests and corresponding to the two databases are described in Fig. 3.

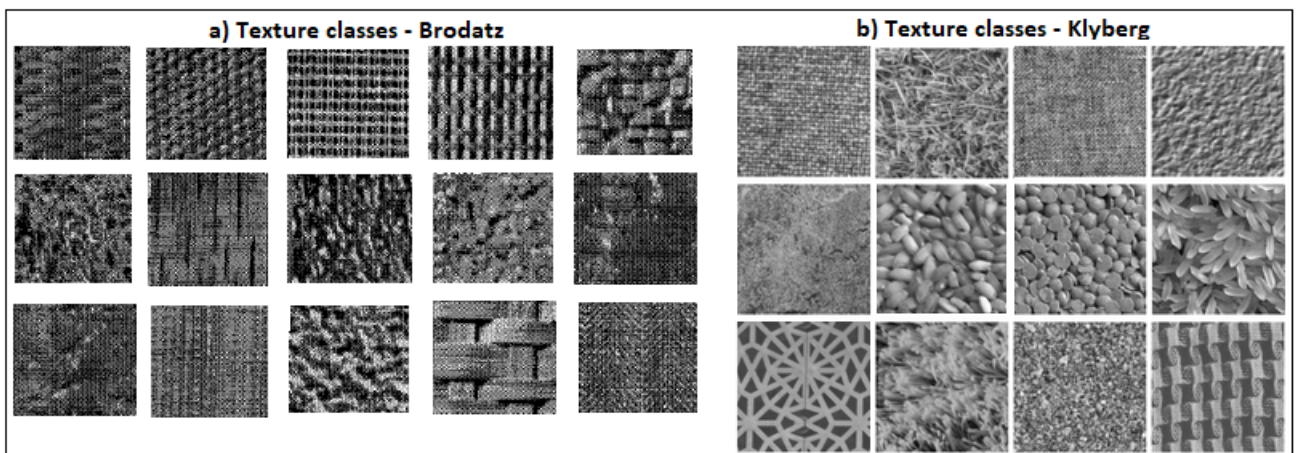


Fig. 3 – Texture classes related to the two databases.

The proposed technique achieves very good texture classification results and high recognition rates in both cases. The confusion matrices corresponding to the recognition experiments performed on the two collections are provided in Table 1 and Table 2. The obtained classification accuracies are 98.7% and 98.4%, since there are only few misclassifications. The overall classification rate of our method is over 98.5%.

Table 1

Confusion matrix corresponding to the tests using Brodatz textures: classification accuracy = 98.7%

	matting	cotton	canvas	cloth	raffia	grass	wood	leather	sand	wool	pigskin	straw	paper	rattan	weave
matting	265														8
cotton		273													
canvas			273												
cloth				273											
raffia					273										
grass						262		6					5		
wood							271				2				
leather								273							
sand									264				9		
wool										262	11				
pigskin											273				
straw							2					271			
paper													273		
rattan														273	
weave												10			263

Table 2

Confusion matrix corresponding to the tests using Kylberg textures: classification accuracy = 98.46%

	blanket	grass	canvas	ceiling	floor1	rice2	lentils1	rice1	floor2	rug	sand	scarf
blanket	225		8									
grass		231				2						
canvas			232								1	
ceiling				227			4				2	
floor1					233							
rice2						229		4				
lentils1							222					
rice1						2		231				
floor2									233			
rug		6			1			8		218		
sand			1	4							228	
scarf												233

Method comparison have been also performed. The proposed multiscale texture recognition approach outperforms other well-known texture analysis methods, such as those based on image moments, LBP features, circularly symmetric 2D Gabor filters and CNN-based circular filters [22], achieving a higher classification accuracy, as one can see in Table 3. Also, our approach runs better for the textures corrupted by additive noise, also.

Table 3

Classification performances of several texture analysis methods

Texture analysis technique	Proposed framework	Moment-based approach	Local Binary Patterns	Circularly symmetric 2D Gabor filters	CNN-based circular filters
Recognition rate	98.5%	87%	91%	97%	95%

However, the described recognition framework is characterized by a high computational complexity, given its anisotropic diffusion-based scale space, GLCM and circular filter components. So, while it achieves high classification accuracies, it may execute slower than other texture analysis algorithms. Its running time depends also on the sizes of the processed texture images. For this reason, the recognition results related to Brodatz album [25] were achieved much faster than those related to the Kylberg database [26]. The

recognition performance of the described multiscale analysis technique could even be improved by increasing the values of some parameters, such as  $K$ ,  $M$ ,  $K_{NN}$  or  $p$ , but the method's complexity and its execution time would become too high if one considers more scales, circular filters, nearest neighbors for the  $K$ -NN classifier or GLCM offsets.

## 5. CONCLUSIONS

We have introduced a new multiscale rotation-invariant texture recognition technique that uses an anisotropic diffusion-based scale space representation and a combined texture descriptor in this work. An important contribution of the described research is the proposed multiscale analysis based on the consistent fast-converging finite difference method-based numerical approximation scheme of a novel compound nonlinear anisotropic diffusion model, which represents a much better solution than 2D Gaussian kernel-based multiscale analysis, since our PDE-based filtering model preserves and enhances the essential image details, overcoming the undesired effects, such as blurring, produced by the classic two-dimension Gaussian filters.

The texture descriptor proposed here, which combines successfully gray-level co-occurrence matrices to 2D circular kernels at multiple scales, provides effective texture analysis results, working properly for textures rotated at various orientations. Our recognition framework achieves a high texture classification accuracy and outperforms many well-known texture recognition methods. It also works properly in noisy conditions.

The recognition approach developed here has a supervised character, applying a  $K$ -NN classifier with a training set to the proposed texture feature vectors. Other supervised learning algorithms, such as those based on artificial neural networks (ANN), could be also used here for texture classification purpose, but an unsupervised version of our recognition technique can be obtained, too. So, the proposed multiscale feature extraction approach can be used in combination to an unsupervised machine learning algorithm, such as  $K$ -means, hierarchical clustering or SOM. Such obtained unsupervised texture recognition solution can be successfully applied in some important texture analysis domains, like texture-based image segmentation and texture indexing and retrieval.

Also, the described multi-scale texture analysis technique can be transformed into a multi-resolution analysis framework, by considering a different resolution for the image at each scale and constructing an anisotropic diffusion pyramid. These multiresolution and unsupervised versions of the proposed recognition framework will represent the focus of our future research in this image analysis field.

## REFERENCES

1. A. FERNANDEZ, M. X. ALVAREZ, F. BIANCONI, *Texture description through histograms of equivalent patterns*, J. Math. Imag. Vis., **45**, 1, pp. 76–102, 2013.
2. M. TUCERYAN, *Moment-based texture segmentation*, Pattern Recognition Letters, **15**, 7, pp. 659–668, 1994.
3. R. M. HARALICK, K. SHANMUGAM, *Textural features for image classification*, IEEE Transactions on Systems, Man, and Cybernetics, **6**, pp. 610–621, 1973.
4. T. OJALA, M. PIETIKAINEN, D. HARWOOD, *A comparative study of texture measures with classification based on featured distributions*, Pattern Recognition, **29**, 1, pp. 51–59, 1996.
5. L. ZHANG, Z. ZHOU, H. LI, *Binary gabor pattern: An efficient and robust descriptor for texture classification*, 2012 19<sup>th</sup> IEEE International Conference on Image Processing, pp. 81–84, September 2012.
6. S. FEKRI-ERSHAD, *Texture classification approach based on energy variation*, International Journal of Multimedia Technology, **2**, 2, pp. 52–55, 2012.
7. H. LIANG, D.S. WELLER, *Edge-based texture granularity detection*, 2016 IEEE International Conference on Image Processing (ICIP), pp. 3563–3567, September 2016.
8. I. EPIFANIO, P. SOILLE, *Morphological texture features for unsupervised and supervised segmentations of natural landscapes*, IEEE Transactions on Geoscience and Remote Sensing, **45**, 4, pp. 1074–1083, 2007.
9. D.G. LOWE, *Distinctive image features from scale-invariant keypoints*, International Journal of Computer Vision, **60**, 2, pp. 91–110, 2004.
10. Y. XU, X. YANG, H. LING, H. JI, *A new texture descriptor using multifractal analysis in multi-orientation wavelet pyramid*, 2010 IEEE Computer Society Conference on Computer Vision and Pattern Recognition, pp. 161–168, June 2010.
11. G.R. CROSS, A.K. JAIN, *Markov random field texture models*, IEEE Transactions on Pattern Analysis & Machine Intelligence, **1**, pp. 25–39, 1983.

12. J. MAO, A.K. JAIN, *Texture classification and segmentation using multiresolution simultaneous autoregressive models*, Pattern Recognition, **25**, 2, pp. 173–188, 1992.
13. A.K. JAIN, F. FAROKHNIA, *Unsupervised texture segmentation using Gabor filters*, Pattern Recognition, **24**, 12, pp. 1167–1186, 1991.
14. S. LIVENS, P. SCHEUNDERS, G. WOUVER, D. van DYCK, *Wavelets for texture analysis, an overview*, 6th International Conference on Image Processing and its Applications, pp. 581–585, 1997.
15. L. SHEN, Q. YIN, *Texture classification using curvelet transform*, Proceedings of the 2009 International Symposium on Information Processing (ISIP 2009), pp. 319, Academy Publisher, 2009.
16. P. YANG, G. YANG, *Feature extraction using dual-tree complex wavelet transform and gray level co-occurrence matrix*. Neurocomputing, **197**, pp. 212–220, 2016.
17. C.M. BISHOP, *Pattern recognition and machine learning*, Springer, 2006.
18. A. VINCENT, P.F. WHELAN, *Using filter banks in convolutional neural networks for texture classification*, Pattern Recognition Letters, **84**, pp. 63–69, 2016.
19. Z. BOULKENAFET, J. KOMULAINEN, X. FENG, A. HADID, *Scale space texture analysis for face anti-spoofing*, 2016 International Conference on Biometrics (ICB), pp. 1–6, June 2016.
20. T. BARBU, A. FAVINI, *Rigorous mathematical investigation of a nonlinear anisotropic diffusion-based image restoration model*, Electronic Journal of Differential Equations, **2014**, 129, pp. 1–9, 2014.
21. T. BARBU, *Variational image inpainting technique based on nonlinear second-order diffusions*, Computers & Electrical Engineering, **54**, pp. 345–353, 2016.
22. P. JOHNSON, *Finite Difference for PDEs*, School of Mathematics, University of Manchester, Semester I, 2008.
23. R. PORTER, N. CANAGARAJAH, *Gabor filters for rotation invariant texture classification*, IEEE International Symposium on Circuits and Systems, Hong Kong, June 9–12, 1997, pp. 1193–1196.
24. P. UNGUREANU, E. DAVID, L. GORAŞ, *On rotation invariant texture classification using two-grid coupled CNNs*, 8<sup>th</sup> Seminar on Neural Network Applications in Electrical Engineering (NEUREL-2006), Belgrade, September 25–27, 2006.
25. P. BRODATZ, *Textures: A photographic album for artists and designers*, Dover, New York, 1966.
26. G. KYLBERG, I. SINTORN, *On the influence of interpolation method on rotation invariance in texture recognition*, J. Image Video Proc., **2016**, p. 17, 2016.

Received July 17, 2020

